27th International Congress of Mechanical Engineering
December 4th–8th, 2023, Florianópolis - SC - Brazil

COB-2023-0118
Numerical Simulation of Ethanol and Hydrogen Peroxide Combustion in a Rocket Chamber

Erykson M. S. Costa
Marcio T. Mendonca
Instituto Nacional de Pesquisas Espaciais
erycksonmarconny@gmail.com, marcio_tm@yahoo.com
Cesar A. V. Salvador
Universidade Federal de Santa Maria
valverde@ufsm.br
Fernando S. Costa
Instituto Nacional de Pesquisas Espaciais
fernando.costa@inpe.br

abstract.
This work uses numerical simulation to investigate the performance of ethanol and hydrogen peroxide as fuel and oxidizer pair for application in a 900 N thruster. Hydrogen peroxide has a relatively high density and is not cryogenic, thus reducing the complexity of the feed system. The numerical model considers the flow of combustion gases and propellant droplets throughout the combustion chamber. The compressible continuity, momentum and energy boundary layer equations are considered for the simulation of the combustion products flow through the chamber. The boundary layer equations are discretized using second order finite differences in the streamwise and radial directions. An evaporation model based on the classic transfer number model computes the droplet evaporation rates of fuel and oxidizer along the combustion chamber, which react and form new products that are then mixed with the pre-existing gases. A chemical equilibrium routine that considers the reaction of ethanol and hydrogen peroxide is used to compute the resulting product composition based on 8 species: CO_2, CO, H_2O, H_2, O_2, H, OH and O. Flow properties and chemical composition along the chamber were determined as a function of equivalence ratio, considering a chamber pressure of 20 atm. Despite the choice of initial equivalence ratio imposed at the injection plate to reduce gas temperatures at the wall region, the local equivalence ratio along the chamber is governed by the evaporation rates of fuel and oxidizer.

keywords: *propulsion, combustion chamber, reactive flow, boundary layer, green propellants*

1. introduction

Green propellants have emerged as a significant area of research in the field of space propulsion. This is due to their notable advantages such as reduced environmental impact, low toxicity, and enhanced safety during transport and storage. By focusing on the development and utilization of green propellants, the aerospace industry can pave the way for a more sustainable and responsible approach to space exploration and satellite deployment. Nowadays, there are numerous research groups working in the characterization and development of various green propellant alternatives. A sample of papers more closely related to the present investigation is presented below.

Mayer and Wieling (2018) presented a study comparing the performance of green propellants and hydrazines (MMH and UDMH) and nitrogen tetroxide (NTO) to find possible alternative propellants that are less toxic and less expensive in terms of handling and storage, but have equal or superior performance. The associate propellant vapor pressure and molar mass, the toxicity level and health risk can be used to quantify the meaning of 'green' in comparing different propellants. Considering a number of requirements based on toxicity and performance for propellant choices, ethanol and hydrogen peroxide is a potential candidate pair for experimental evaluation and identification of technology gaps that need to be addressed in the development of green propellants. Considering the pair ethanol and hydrogen peroxide, ignition may be initiated by either an external igniter, catalytic decomposition or by hypergolic ignition with the help of dissolved catalyst in the ethanol. Their study found that the best ignition method is the last one, using catalyst to obtain a hypergolic reaction, which was successfully reproduced in the tests. However, the combustion was irregular and it was not possible to obtain accurate results in order to evaluate the propellant performance and further optimization of the propellant mixture is necessary.

Before that, in 2017, Indiana *et al.* (2017) investigated the combustion of ethanol and hydrogen peroxide in order to evaluate combustion performance and characterize their atomization and combustion. They opted for non-hyperbolic, non-

catalytic combustion and ignited the propellants with a thermal torch. They evaluated both triplet and doublet impinging injectors in order to verify the possibility of achieving a shorter mixing length. They concluded that the triplet spray has a more homogeneous properties and better mixing than doublet sprays which also has lifted off flame as opposed to an anchored flame of the triplet spray. The performance of the triplet injector also results in a shorter combustion length.

In subsequent publications, Indiana *et al.* (2019) and Boust and Bellenoue (2019) presented studies examining different injection mechanisms to access the differences between separate atomization of fuel and oxidizer, as opposed to atomizing both reactants already combined and also the atomization and combustion processes. Separate and combined injection are obtained with like-doublet and unlike-triplet injectors, respectively. In separate atomization, each reactant has to undergo atomization, vaporization, mixing and chemical reaction, increasing the combustion chamber volume. In the second option a single spray with both propellants has only to vaporize before burning. Combustion efficiencies are compared for equivalence ratios in a range from 0.5 to 2.2. The proposed injector configurations were chosen to investigate nonhypergolic reaction performance for liquid propellants, with hydrogen peroxide without previous decomposition in a catalytic bed.

The combustion characteristics of hydrogen peroxide as oxidizer and RP-1, methane and ethanol as fuels have been studied by Gorakula *et al.* (2021). They investigated combustion temperatures, combustion gases composition and specific impulse at different equivalence ratios and chamber pressures using the CEA-NASA code. They observed that hydrogen peroxide concentration has a significant effect on the combustion performance, but a minor effect on the specific impulse. Regarding combustion gases composition, water vapor is the most prevalent product followed by carbon dioxide and carbon monoxide. Lower equivalence ratios result in lower temperatures.

In order to study flame stability and engine performance, Wang et al. (Wang *et al.*, 2021) developed a liquid rocket engine burning ethanol and hydrogen peroxide with 2000 N thrust with combustion chamber pressure of 20 bar. The hydrogen peroxide is decomposed in a catalytic bed and mixed with ethanol in an impinging injector with multiple jets. To increase mixing they proposed a backward facing step to create a recirculation zone that increases the reactants residence time in the combustion chamber. The fuel and oxidizer mass flow rates and geometry are equivalent to the present study. Their specific impulse is in the range of 200 seconds.

A up-to-date literature review presents recent publications related to different hypergolic systems using hydrogen peroxide as oxidizer (Turker, 2023). The manuscript shows the strong increase in research related to green propellants, in particular related to hydrogen peroxide. The authors concluded that new propellants should yield high specific impulse, low ignition delay, stable combustion with safer handling and lower toxicity than previous propellants used in rocket engines.

This article presents the results of an ongoing development of a two-dimensional numerical model that simulates the combustion of ethanol and hydrogen peroxide in a rocket engine's combustion chamber. The primary objective is to create a numerical tool to assist in the design and performance analysis of combustion chambers. Additionally, the model seeks to enable further characterization of environmentally friendly propellants, with the added flexibility of easily incorporating other propellants by substituting physical and thermodynamic properties subroutines.

2. Methods

2.1 Engine Parameters

The engine parameters were determined with the help of the CEA-NASA (2004) code, for stoichiometric combustion of ethanol and hydrogen peroxide, assuming a chamber pressure of 20 atm (2.026500×10^6 Pa) and a nozzle expansion ratio of 100. The theoretical equilibrium vacuum specific impulse is I_s = 360 s.

Considering a thrust level of 900 N and a standard gravity acceleration of $g_0 = 9.8066$ m/s^2, the propellant mass flow rate $\dot{m}$ is

$$I_s = \frac{F}{\dot{m} g_0} \quad \rightarrow \quad \dot{m} = 0.2549 \text{ kg/s}. \tag{1}$$

Considering a reference value for the equivalence ratio $\phi = 1$, and that the stoichiometric fuel to air mass flow ratio $f = \dot{m}_f / \dot{m}_o$ is equal to 0.2257, the mass flow of fuel and oxidizer, $\dot{m}_f$ and $\dot{m}_o$ respectively, result

$$\dot{m} = \dot{m}_f + \dot{m}_o, \tag{2}$$

$$f = \frac{\dot{m}_f}{\dot{m}_o}, \tag{3}$$

$\dot{m}_f = 0.0469$ kg/s and $\dot{m}_o = 0.2080$ kg/s.

The throat area A_t may be estimated from the propellant mass flow rate using $c^* = PA_t/\dot{m}$, The effective exhaust velocity c is given by

$$c = \frac{F}{\dot{m}} = 3503.8 \text{ m/s}, \tag{4}$$

and the characteristic velocity c^* calculated by the CEA-NASA code is 1670 m/s.

Therefore, the throat area is given by

$$A_t = \frac{\dot{m}c^*}{p} = 2.1 \times 10^{-4} \text{ m}^2 \tag{5}$$

such that the throat diameter is

$$d_t = \sqrt{\frac{4A_t}{\pi}} = 1.6352 \times 10^{-2} \text{ m}, \tag{6}$$

Choosing the chamber diameter $d_c = 3.1 \times 10^{-2}$ m, such that $d_c/d_t \approx 2$, results in a combustion chamber area $A_c = 7.5477 \times 10^{-4}$. The resulting combustion chamber to throat area ratio A_c/A_t is equal to 3.5941, which is between three and four, the recommended range to reduce pressure losses.

An estimate for the chamber length can be obtained from the characteristic length L^*, from which the characteristic chamber volume V_c could be computed.

$$L^* = \frac{V_c}{A_t}, \tag{7}$$

where typical values are in the range $64 \leq L^* \leq 152$ cm.

Assuming an combustion chamber length $L = 17.02$ cm, the combustion chamber volume is equal to

$$V_c = A_c L + A_c(0.1L)\left(1 + \sqrt{A_t/A_c} + A_t/A_c\right) = 1.7098 \times 10^{-4} \text{ m}^3, \tag{8}$$

where the chamber volume includes both the constant area region of the combustion chamber and the convergent part of the nozzle, which is usually about 10% of the length of the combustion chamber Sutton and Biblarz (2017). The resulting characteristic length is $L^* = 81.42$ cm, that is within the range of typical values.

The chamber length value will be compared to the length necessary to evaporate the fuel and oxidizer droplets.

For these data the thrust coefficient C_f is equal to

$$C_f = \frac{F}{A_t p} = 2.1148, \tag{9}$$

which is close to 2, as expected from typical values.

2.2 Numerical Model

A schematic drawing of a combustion chamber is presented in Fig. 1 (Salvador and Costa, 2006). The process in the combustion chamber comprises four phases: 1) injection of fuel and oxidizer droplets with known size distribution and injection of fuel and oxidizer vapors; 2) vaporization of fuel and oxidizer droplets; 3) combustion of fuel and oxidizer vapors; and 4) mixing with pre-existing combustion products.

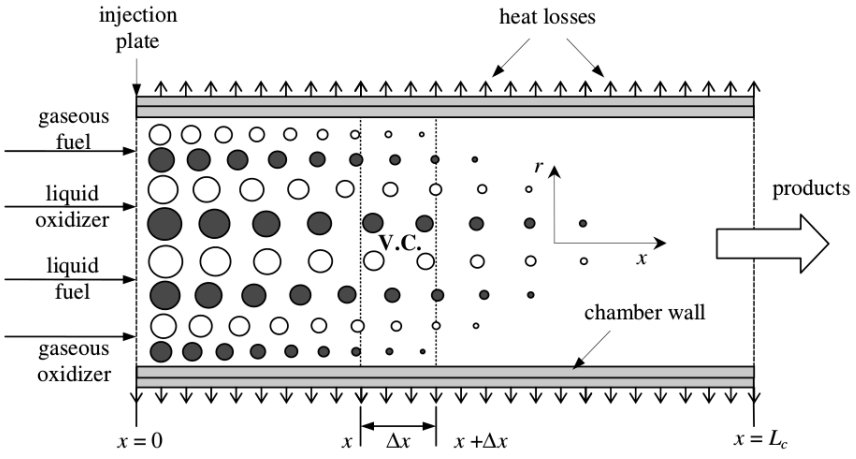

Figure 1. Combustion chamber model (Salvador and Costa, 2006).

Mass, momentum and energy balance equations are solved, given initial conditions at the combustion chamber entrance. The following simplifying assumptions are considered:

1. two-dimensional axisymmetric, constant cross section combustion chamber;
2. steady state condition;
3. laminar flow;
4. process controlled by vaporization of droplets, with combustion reaction much faster than vaporization;
5. no volume forces, such as gravity forces;
6. Soret and Dufour effects negligible;
7. negligible viscous dissipation;
8. no mass diffusion between neighbour volumes in the radial direction;
9. negligible radial pressure gradient;
10. heat, mass and momentum diffusion in the streamwise direction negligible, leading to boundary layer type equations.

2.2.1 Balance equations

The two-dimensional, axisymmetric continuity, momentum and energy equations with boundary layer approximation in cylindrical coordinates are (Kuo, 1986):

Continuity equation:

$$\frac{1}{r}\frac{\partial}{\partial r}\left(\rho r u_r\right) + \frac{\partial}{\partial z}\left(\rho u_z\right) = 0, \tag{10}$$

where, r and z are the radial and axial coordinates, ρ is the density, u_r and u_z are the radial and streamwise velocity components, respectively.

Streamwise and radial momentum equations:

$$\rho u_r \frac{\partial u_z}{\partial r} + \rho u_z \frac{\partial u_z}{\partial z} = -\frac{\partial p}{\partial z} + \frac{1}{r}\frac{\partial}{\partial r}\left(r\mu\frac{\partial u_z}{\partial r}\right), \tag{11}$$

$$\frac{\partial p}{\partial r} = 0, \tag{12}$$

where p is the pressure and μ stands for the dynamic viscosity coefficient.

Energy balance equation:

$$\rho c_p\left(u_r\frac{\partial T}{\partial r} + u_z\frac{\partial T}{\partial z}\right) - u_z\frac{\partial p}{\partial z} = \frac{1}{r}\frac{\partial}{\partial r}\left(kr\frac{\partial T}{\partial r}\right), \tag{13}$$

where c_p is the specific heat at constant pressure, k is the thermal conductivity coefficient and T stands for temperature.

Perfect gas equation of state:

$$p = \rho R_u T \sum_{i=1}^{N}\frac{Y_i}{W_i}, \tag{14}$$

where R_u is the universal gas constant Y_i and W_i are the mass fraction and molar mass of species i. The mole fraction is related to the mass fraction by

$$X_i = \frac{Y_i/W_i}{\sum_j\left(Y_j/W_j\right)}, \tag{15}$$

where X_i is the mole fraction of species i

2.2.2 Initial and boundary conditions

The parabolic boundary layer equations are integrated downstream from initial conditions given at the injection plate position. Boundary conditions are imposed at the combustion chamber centerline and at the chamber wall.

The initial conditions are given at the injection plate combustion chamber entrance as shown in Fig. 1. Liquid fuel and oxidizer are introduced at the injection plate with a known droplet sizes and mass flow rates. Part of the fuel and oxidizer mass flow rates (10% w/w) are considered as already vaporized and reacted at the inlet boundary, such that a mass flow rate of pre-existing gases is specified. At this inlet boundary uniform initial conditions for the pre-existing gases velocity and temperature are given ($u_z = U_0, u_r = 0, T = T_0$). The inlet velocity U_0 is based on the given mass flow rate of pre-existing gas and combustion chamber cross-section area. The inlet gas temperature T_0 is specified as an input parameter or computed as the equilibrium temperature of the combustion reaction for the given ratio of fuel to oxidizer mass flow rates $\dot{m}_f/\dot{m}_{ox}$.

At the chamber wall zero velocity, no slip, boundary condition and adiabatic wall are imposed. At the centerline of the combustion chamber symmetry conditions for the velocity components $du_z/dr = 0, u_r = 0$ and adiabatic centerline condition $dT/dr = 0$ are applied.

2.2.3 Solution procedure

The boundary layer equations presented above are solve numerically marching in the streamwise direction from given initial conditions. At each streamwise position the boundary layer equations are solved numerically for the velocity and temperature distributions with a second order finite differences backward scheme in the streamwise direction and a second order centered finite differences scheme in the radial direction.

The gas composition and properties lag behind from the previous marching step. Given the velocity and temperature fields at each computed streamwise position, the fuel and oxidizer evaporation and reaction are then computed. Liquid propellant evaporation are computed according to the methodology of Chin and Lefebvre (1983) and Lefebvre and McDonell (2017).

Thermodynamic and physical properties are computed based on correlations found on the National Institute of Standards and Technology (NIST) website (https://www.nist.gov/) and NASA Chemical Equilibrium Applications program (CEA) (https://cearun.grc.nasa.gov/). Specific heat and enthalpy are evaluated from the polynomials from McBride *et al.* (1993). Physical properties results from kinetic theory for gases (Law, 2006) and other sources (Svehla, 1995; Poling *et al.*, 1977).

The combustion products are a mixture of the eight species considered in the reaction. Chemical equilibrium conditions are determined for the reaction of C_2H_5OH and H_2O_2 resulting in 8 chemical species: CO_2, CO, H_2O, H_2, O_2, H, OH and O.

Details of the physical properties model may be found on Law (2006). Liquid fuel and oxidizer propellant properties are evaluated from correlations taken from the NIST and CEA-NASA , where correlations for vapor pressure based on Antoine equation and vaporization enthalpy are also available.

The combustion products from the evaporated reactants are then mixed with the pre-existing gases coming from the upstream position in a thermodynamic equilibrium and mass conservation routine to compute the mixture temperature, mass flow rate and gas velocity. The process is repeated for each radial finite difference position until the fuel or oxidizer droplets are completely evaporated.

To start the computation, the geometry of the combustion chamber, the fuel and oxidizer inlet areas and total mass flow rates are given, along with the liquid propellants temperature, combustion chamber pressure and amount of propellants already reacted at the chamber entrance, simulating a recirculation of gases in the combustion chamber.

2.2.4 Verification and Grid Convergence Tests

The boundary layer solver has been verified and validated against analytical results for inert flow on a channel. Grid refinement tests have also been performed to ensure grid independent results.

Figure 2 shows a comparison of the computed streamwise velocity radial distribution with the analytic parabolic velocity profile, showing good agreement. At the combustion chamber inlet a uniform velocity distribution was specified and marched downstream. At the end of the combustion chamber the velocity profile has evolved to the expected fully developed parabolic laminar velocity distribution.

The verification of the chemical equilibrium routine was performed comparing results with results obtained from CEA-NASA. Results are presented in Tab. 1 in terms of equilibrium temperature and mole fraction for different species and three different equivalence ratios, $\Phi = 0.2, 1.0$ and 5.

The droplets evaporation routine was validated considering the steady state equilibrium droplets temperatures and the droplets evaporation rates for chamber pressures of 10 and 20 atm. Figure 3 shows the evolution of the fuel (T_f) and oxidizer (T_{ox}) droplets temperatures versus distance x from the injection plate. After an initial transient region, where the

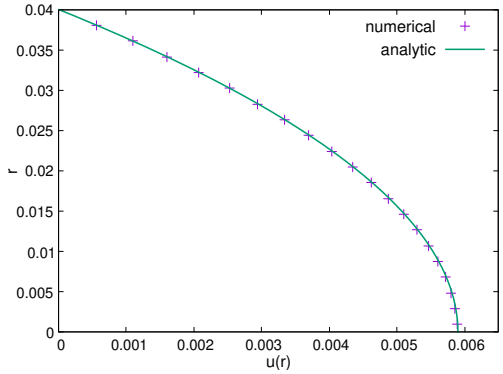

Figure 2. Comparison between numerical velocity profile with analytic parabolic velocity profile.

Table 1. Results from the chemical equilibrium routine in terms of equilibrium temperature and composition for three different equivalence ratios.

equivalence ratio	0.2	0.2	1	1	5	5
	Model	CEA	Model	CEA	Model	CEA
T [K]	3328	3325	3523	3520	2734	2733
M [g/mol]	20.89	20.89	18.95	18.95	13.94	13.94
X(CO2)	0.02691	0.02675	0.0605	0.06014	0.0196	0.01944
X(CO)	0.01226	0.01242	0.0909	0.09132	0.3012	0.30134
X(H2O)	0.5478	0.54679	0.5102	0.50956	0.2037	0.20384
X(H2)	0.03142	0.03171	0.0929	0.09310	0.4645	0.46428
X(O2)	0.2150	0.21471	0.0595	0.05962	2.5014E-6	< 1.E-5

droplets are heated by the combustion gases at high temperatures, the droplets reach a steady state temperature close to the boiling temperature. For ethanol the boiling temperatures at 10 and 20 atmospheres are 425 and 454 K. For hydrogen peroxide they are 508 and 541 K, respectively. The corresponding steady state temperatures are $T_f(p = 10 \text{ atm}) = 415$ K and $T_f(p = 20 \text{ atm}) = 445$ K for the ethanol and $T_{ox}(p = 10 \text{ atm}) = 497$ K and $T_{ox}(p = 20 \text{ atm}) = 532$ K for the hydrogen peroxide. These results are in agreement with the expected theoretic values (Lefebvre and McDonell, 2017).

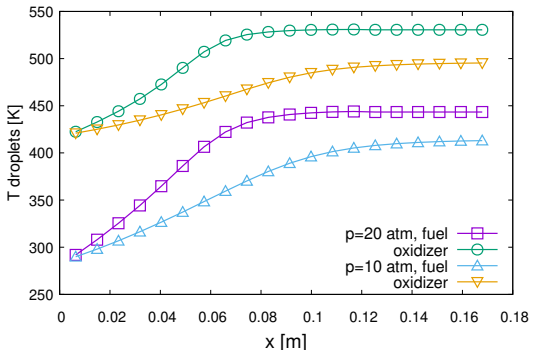

Figure 3. Ethanol and hydrogen peroxide droplets temperature variation along the combustion chamber for chamber pressures equal to 10 and 20 atm.

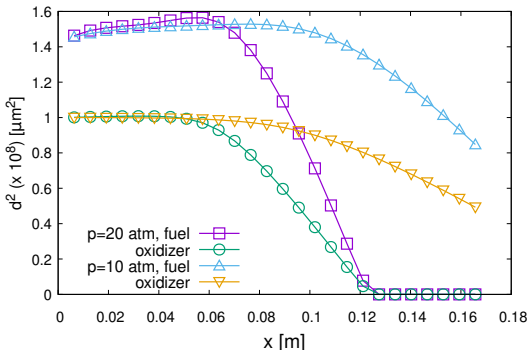

Figure 4. Ethanol and hydrogen peroxide droplets diameter squared variation along the combustion chamber for chamber pressures equal to 10 and 20 atm.

In the steady state regime the droplet diameter should vary according to the diameter square law (Lefebvre and McDonell, 2017), which predicts that the square of the droplet diameter should vary linearly downstream along the combustion chamber. Figure 4 shows the variation of the fuel and oxidizer droplets diameters square, where after the unsteady droplets warm-up period the droplets diameter square varies linearly as expected. During the warm-up period the droplets diameters do not vary significantly since the reduction in diameter is compensated by an increase due to droplet dilatation with increasing temperature.

3. RESULTS

The combustion chamber under consideration is divided in two regions, a core region comprising about 80% of the chamber diameter and a wall region comprising the remaining 20%. The total equivalence ratio is defined as the equivalence ratio given by the total mass flow ratio of fuel and oxidizer at the injection plate. Local equivalence ratios are the equivalence ratios due to the evaporated masses from fuel and oxidizer droplets.

At the core region the total equivalence ratio is kept equal do 1. At the wall region three values of total equivalence ratio are imposed, $\Phi = 1, 0.2$ and 5. The equivalence ratio at the wall region is changed by changing the mass flow rate of fuel and keeping the same mass flow rate of oxidizer as that of the core region. The resulting reduction in total mass flow rate when $\Phi = 0.2$ close to the wall, results in a theoretical thrust of 856.8 N according to Eq. (1). When $\Phi = 5$ close to the wall the increased mass flow rate results in a theoretical thrust of 1112.4 N.

The main parameter of interest in the present study is the combustion gases temperature at the wall region, which is important for wall cooling design and combustion chamber integrity.

Based on the analysis of Sec. 2.1 the following parameters are considered for the combustor burning ethanol and hydrogen peroxide:

- combustion chamber diameter $D_i = 31$ mm and length $L = 170$ mm;
- total oxidizer mass flow rate $\dot{m}_{ox} = 208$ g/s;
- oxidizer mass flow rate evaporated at the inlet to form the pre-existing gases 10% of $\dot{m}_{ox}$;
- equivalence ratio imposed to compute the fuel mass flow rate for the pre-existing gases $\Phi = 1.0$;
- equivalence ratio imposed to compute the liquid fuel mass flow rate at the core region, $\Phi = 1.0$;
- equivalence ratios imposed to compute the liquid fuel mass flow rate at the wall region, $\Phi = 1, 0.2$ and 5;
- initial liquid fuel and oxidizer droplets temperature of $T_f = 288$ K; and $T_{ox} = 420$ K, respectively;
- initial liquid fuel and oxidizer droplets diameter of $d_f = 120$ μm and $d_{ox} = 100$ μm, respectively;
- chamber pressure $P_0 = 20$ atm.

3.1 Droplets Diameter

Figure 5 shows the variation of the droplet diameter versus distance along the chamber. For all test conditions the fuel droplets diameter initially increases due to heating by the hot gaseous product, after which the diameter decreases due to evaporation. For the hydrogen peroxide, initially the thermal expansion is balanced by the evaporation such that the droplets diameter remains constant. After the initial expansion the evaporation rate results in a linear variation of the droplet diameter squared, as expected. Fuel and oxidizer at the core region are consumed at a rate such that both totally evaporate at the same chamber streamwise location. Close to the wall, there is a residual oxidizer after the fuel was totally consumed and the evaporation of the remaining oxidizer is no longer computed in the present version of the numerical model.

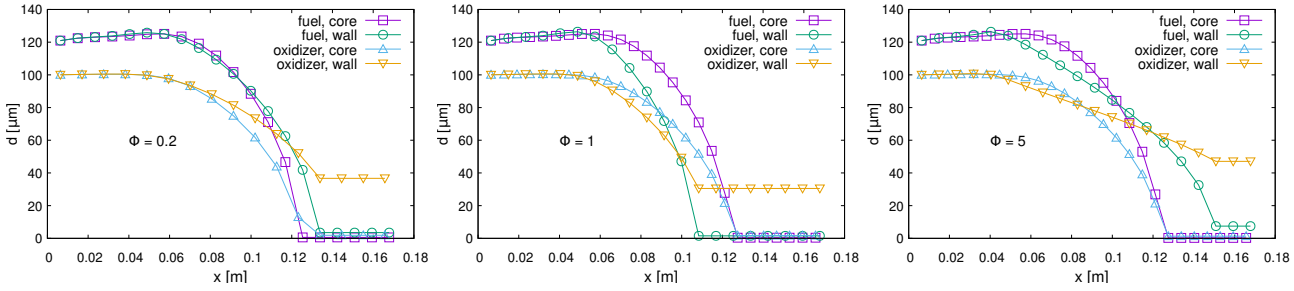

Figure 5. Droplets diameter along the chamber for different equivalence ratios (Φ) near the chamber wall.

The evaporation rate of fuel and oxidizer close to the wall varies significantly with the variation of the total equivalence ratio. The higher evaporation rates are observed when $\Phi = 1$, as expected, since higher temperatures are observed for this equivalence ratio. Even for $\Phi = 1$ the evaporation rates are not the same at the core and wall regions because the evaporation rate depends on the radial temperature distribution of the combustion gases, which depends on the near wall boundary layer conditions. The evaporation rates are also dependent on the droplet velocities, since the residence time of

the droplet in a given small control volume used to compute evaporation determines the time available for evaporation. Changing the fuel mass flow rate close to the wall for different equivalence ratios, changes both the combustion gases temperature and droplet speeds. As another consequence, the change in the evaporation rates also changes the local equivalence ratio, which also affects the combustion gases temperature.

3.2 Droplets Temperature

The temperatures of the fuel and oxidizer droplets increase downstream from the given initial temperature, as shown in Fig. 6, caused by heat transfer from the combustion gases. After the initial increase of the droplets temperature due to heating by the hot gaseous products, the droplets temperature remains constant and close to the boiling temperature (wet bulb temperature). The lower temperatures observed close to the wall for $\Phi = 5$ are due to the lower combustion gases temperature at this equivalence ratio, as shown in Fig. 7. The hot gases temperature along the chamber also explains the differences between the core and wall region, which depend on the total equivalence ratio and local equivalence ratio. The local equivalence ratio is a consequence of the different evaporation rates of fuel and oxidizer.

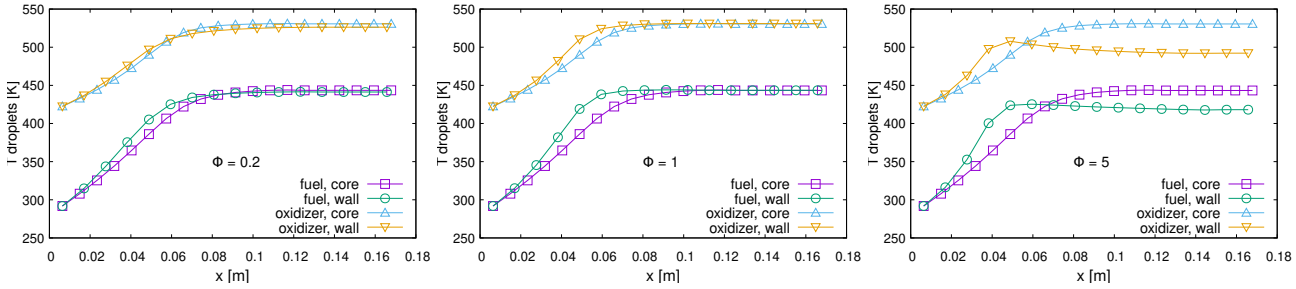

Figure 6. Droplets temperature along the chamber for different equivalence ratios Φ near the chamber wall.

3.3 Gas Temperature

The downstream temperature variation of the gaseous products along the chamber is shown in Fig. 7. As can be seen, the gaseous products temperature is a strong function of both the total equivalence ratio and the local equivalence ratio controlled by the evaporation rates. Close to the wall, for equivalence ratios $\Phi = 0.2$ and 5, the reaction equilibrium temperatures are lower, affecting droplet heating (Fig. 6), droplet evaporation rates (Fig. 9) and local equivalence ratios due to evaporation (Fig. 8).

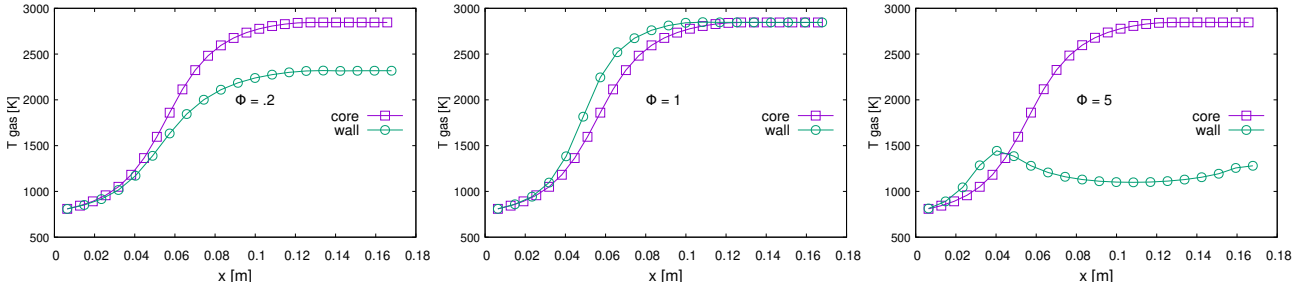

Figure 7. Combustion gases temperature along the chamber for different equivalence ratios Φ near the chamber wall.

3.4 Equivalence Ratio

The local equivalence ratios, shown in Fig. 8, are determined by the evaporation rates of fuel and oxidizer. For total equivalence ratios equal do 0.2 and 5, the local equivalence ratios close to the chamber wall are far from stoichiometric due to significant differences in fuel and oxidizer evaporation rates. The resulting near wall temperatures are lower, as required for chamber wall integrity.

3.5 Mass Flow rate

Figure 9 shows the mass flow rates of liquid fuel and liquid oxidizer for the three equivalence ratios near the chamber wall considered in the present study. The mass flow rates of liquid fuel and liquid oxidizer decrease along the chamber due to the evaporation of the droplets. In the core region the mass flow rates of fuel and oxidizer are the same for all

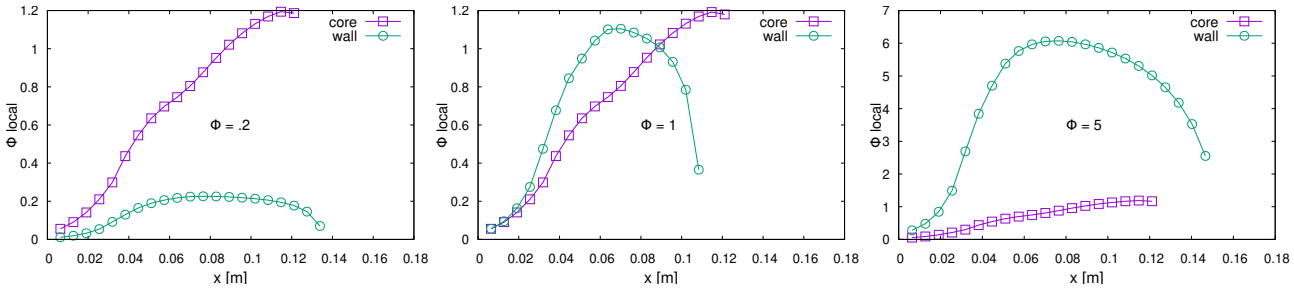

Figure 8. Local equivalence ratio due to evaporation along the chamber for different equivalence ratios near the chamber wall.

three different equivalence ratios considered close to the wall. In the wall region the lower equivalence ratio, $\Phi = 0.2$, corresponds to a reduced fuel mass flow rate for a fixed oxidizer mass flow rate, while the higher equivalence ratio, $\Phi = 5$, corresponds to an increased fuel mass flow rate near the wall. The liquid propellants mass flow rates vary with the evaporation rates. These liquid propellants mass flow rates are higher downstream for $\Phi = .2$ and 5 due to the lower values of the temperatures of the gaseous products which reduce the evaporation rates.

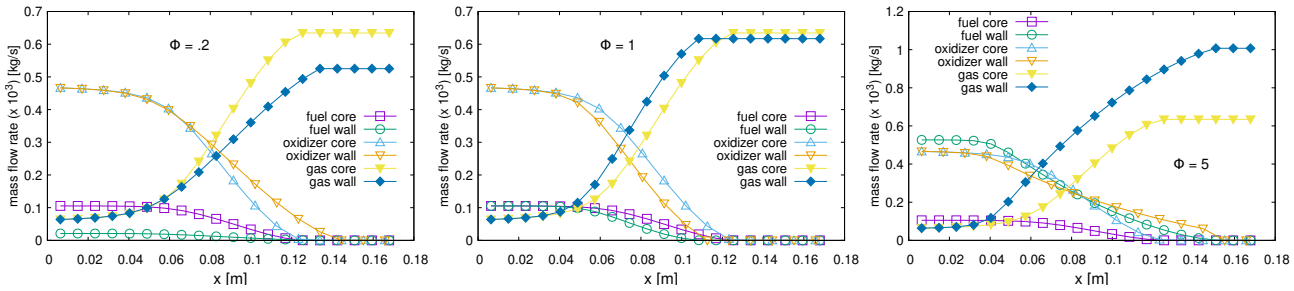

Figure 9. Liquid fuel and oxidizer mass flow rate along the chamber at the core and wall regions, for different equivalence ratios near the chamber wall.

The equivalence ratio in the wall region, with stoichiometric, fuel lean and fuel rich values, influences significantly the mass flow rates and the temperatures of gaseous products. The initial equivalence ratios at the core and near the chamber wall define the temperatures of combustion gases. This temperature, in turn, defines the evaporation rates and local equivalence ratios (Fig. 8).

3.6 Mole Fraction

Mole fraction for CO_2, CO, H_2O, H_2 and O_2 are shown in Figs 10 and 11. Mole fraction of each species depends mostly on the equivalence ratios, with reduction of CO_2 for non-stoichiometric mixtures and significant increase of CO and H_2 and reduction in water vapor for fuel rich mixtures.

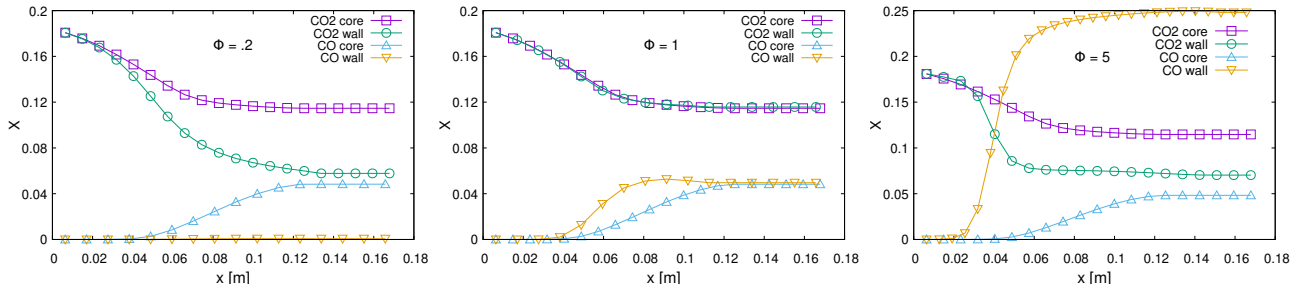

Figure 10. CO_2 and CO mole fraction X along the chamber at the core and wall regions, for different equivalence ratios near the chamber wall.

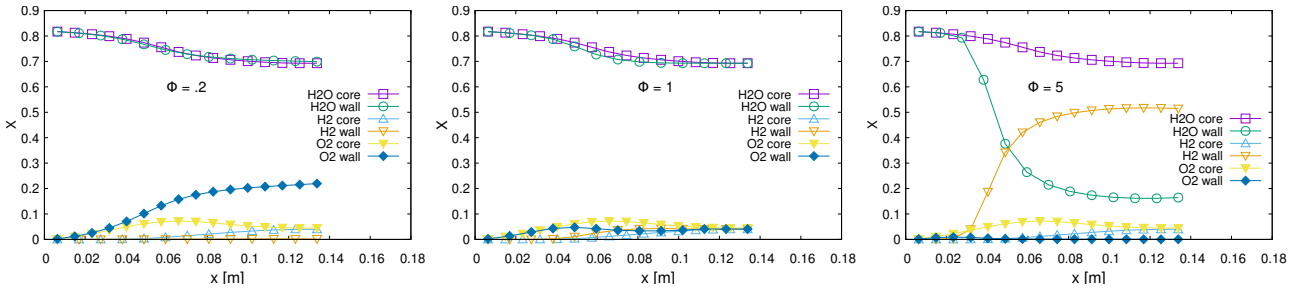

Figure 11. H_2O, H_2 and O_2 mole fraction X along the chamber at the core and wall regions, for different equivalence ratios near the chamber wall.

4. CONCLUSIONS

The spray combustion of ethanol and hydrogen peroxide was simulated by a new two dimensional axisymmetric numerical code based on the boundary layer equations. The variations of droplet diameters, droplet temperatures, gas temperature, equivalence ratio due to evaporation, mass flow rates and combustion gases composition along the chamber were described. By changing the initial equivalence ratio close to the wall it was possible to change the combustion gases temperatures and, as a consequence, change the evaporation rates and the local equivalence ratio. The model presents consistent results with expected combustion behaviour in terms of temperatures and combustion gas composition. These results are valid up to the streamwise position where one of the reactants completely evaporates. At that position, the evaporation of the remaining component is no longer computed. An improvement to the present model is under development, where the remaining reactant will evaporate and decompose under the effect of high temperature from the combustion gases, changing the final mixture temperature downstream.

5. REFERENCES

Boust, B. and Bellenoue, M., 2019. "Atomization and combustion of a single unlike-triplet spray of storable bipropellants: Hydrogen peroxide with ethanol or alkanes". In *8th European Conference for Aeronautics and Space Sciences – EUCASS*. Madrid, Spain. doi:10.13009/EUCASS2019-279.

Chin, J.S. and Lefebvre, A.H., 1983. "Steady-state evaporation characteristics of hydrocarbon fuel drops". *AIAA Journal*, Vol. 21, No. 10, pp. 1437–1443.

Gorakula, S., Bondugula, M.S.R., Patel, S. and Inapanury, A., 2021. "Hydrogen peroxide vs liquid methante: Green birpropellants for future space propulsion applications". *International Journal of Scientific and Research Publications*, Vol. 11, No. 8, pp. 328–335. doi:10.29322/IJSRP.11.08.2021.p11643.

Indiana, C., Boust, B., Bellenoue, M. and Azuma, N., 2017. "Combustion of sprays from triplet injector with green propellants: ethyl alcohol and hydrogen peroxide". In *7th European Conference for Aeronautics and Space Sciences – EUCASS*. Milan, Italy. doi:10.13009/EUCASS2017-233.

Indiana, C., Boust, B., Bellenoue, M. and Azuma, N., 2019. "Effect of injector design on the combustion of ethanol and hydrogen-peroxide sprays". *Journal of Propulsion and Power*, Vol. 35, No. 3, pp. 1–10. doi:10.2514/1.B37286.

Kuo, K.K., 1986. *Principles of Combustion*. Wiley-Interscience, John Wiley & Sons, Inc., New York.

Law, C.K., 2006. *Combustion Physics*. Cambridge University Press.

Lefebvre, A.H. and McDonell, V.G., 2017. *Atomization and Sprays*. CRC Press, Taylor and Francis Group, 2nd edition.

Mayer, A. and Wieling, W., 2018. "Green propulsion research at tno the netherlands". *Transations of the Institute of Aviation*, Vol. 4, No. 253, pp. 1–24. doi:10.2478/tar-2018-0026.

McBride, B.J., Gordon, S. and Reno, M.A., 1993. "Coefficients for calculating thermodynamic and transport properties of individual species". Reference publication 4513, National Aeronautics and Space Administration, National Aeronautics and Space Administration. Lewis Research Center. Cleveland, Ohio 44135.

Poling, B.E., Prausnitz, J.H. and O'Connell, J.P., 1977. *The Properties of Gases and Liquids*. The McGraw-Hill Companies, Inc. McGraw Hill Book Company, 5th edition.

Salvador, C.A.V. and Costa, F.S., 2006. "Vaporization lengths of hydrazine fuels burning wih nto". *Journal of Propulsion and Power*, Vol. 22, No. 6, pp. 1362–1372.

Sutton, G.P. and Biblarz, O., 2017. *Rocket Propulsion Elements*. John Wiley & Sons, Inc., New Jersey, USA, 9th edition. ISBN 9781118753651.

Svehla, R.A., 1995. "Transport coefficients for the nasa lewis chemical equlibrium program". Technical Memorandum 4647, NASA, National Aeronautics and Space Administration. Lewis Research Center. Cleveland, Ohio 44135.

Turker, L., 2023. "Hypergolic systems based on hydrogen peroxide". *Earthline Journal of Chemical Sciences*, Vol. 10,

No. 1, pp. 1–42. doi:10.34198/ejcs.10123.142.

Wang, Y.K., Lin, Y.T., Wei, S.S. and Wu, J.S., 2021. "Development of a 20 kgf class liquid rocket engine by using hydrogen peroxide and ethanol". In *International Conference on Astronautics and Space Exploration (iCASE)*. Taiwan National Space Organization, Taiwan Space Industry Development Association, NSPO-TSIDA, Hsinchu, Taiwan.